# The Role of G$\beta\gamma$ and Domain Interfaces in the Activation of G Protein-Coupled Receptor Kinase 2†

David T. Lodowski,‡ Jennifer F. Barnhill,‡ Robyn M. Pyskadlo,§ Rodolfo Ghirlando,|| Rachel Sterne-Marr,§ and John J. G. Tesmer*,‡

*Department of Chemistry and Biochemistry, Institute for Cellular and Molecular Biology, The University of Texas at Austin, 1 University Station #A5300, Austin, Texas 78712-0165, Laboratory of Molecular Biology, National Institute of Diabetes and Digestive and Kidney Diseases, National Institutes of Health, Department of Health and Human Services, Bethesda, Maryland 20892-0540, and Biology Department, Siena College, 123 Morrell Science Center, 515 Loudon Road, Loudonville, New York 12211*

*Received January 20, 2005; Revised Manuscript Received March 8, 2005*

ABSTRACT: In response to extracellular signals, G protein-coupled receptors (GPCRs) catalyze guanine nucleotide exchange on Gα subunits, enabling both activated Gα and G$\beta\gamma$ subunits to target downstream effector enzymes. One target of G$\beta\gamma$ is G protein-coupled receptor kinase 2 (GRK2), an enzyme that initiates homologous desensitization by phosphorylating activated GPCRs. GRK2 consists of three distinct domains: an RGS homology (RH) domain, a protein kinase domain, and a pleckstrin homology (PH) domain, through which it binds G$\beta\gamma$. The crystal structure of the GRK2−G$\beta\gamma$ complex revealed that the domains of GRK2 are intimately associated and left open the possibility for allosteric regulation by G$\beta\gamma$. In this paper, we report the 4.5 Å structure of GRK2, which shows that the binding of G$\beta\gamma$ does not induce large domain rearrangements in GRK2, although small rotations of the RH and PH domains relative to the kinase domain are evident. Mutation of residues within the larger domain interfaces of GRK2 generally leads to diminished expression and activity, suggesting that these interfaces are important for stability and remain intact upon activation of GRK2. Geranylgeranylated G$\beta\gamma$, but not a soluble mutant of G$\beta\gamma$, protects GRK2 from clostripain digestion at a site within its kinase domain that is 80 Å away from the G$\beta\gamma$ binding site. Equilibrium ultracentrifugation experiments indicate that neither abnormally large detergent micelles nor protein oligomerization can account for the observed protection. The G$\beta\gamma$-mediated binding of GRK2 to CHAPS micelles or lipid bilayers therefore appears to rigidify the kinase domain, perhaps by encouraging stable contacts between the RH and kinase domains.

G protein-coupled receptors (GPCRs)[1] are integral membrane proteins that relay external signals into the cytoplasm of the cell. In order for cells to adapt to changes in their extracellular environment, activated GPCRs are desensitized. A well-characterized system for desensitization that appears to operate on nearly every GPCR is that of the G protein-coupled receptor kinases (GRKs) and arrestins (*1*−*3*). GRKs catalyze the phosphorylation of serine and threonine residues on the cytoplasmic loops or tails of activated GPCRs. These phosphorylated receptors are then bound by molecules of arrestin, which block the access of heterotrimeric G proteins to the receptors (*4*, *5*), target the receptors for clathrin-mediated endocytosis (*1*, *6*), and serve as adaptors that link receptors to other signaling pathways such as those of the MAP kinases (*7*, *8*).

GRK2 was initially identified by its ability to phosphorylate agonist-occupied $\beta_2$-adrenergic receptors (*9*, *10*). Through its regulation of cardiac receptors, GRK2 plays key roles in both the healthy and failing heart and has been implicated as an important drug target for treatment of congestive heart failure and tissue ischemia (*11*, *12*). Like other GRKs, the activity of GRK2 is enhanced by as much as several orders of magnitude in vitro upon binding activated receptors (*13*−*15*). However, GRK2 activity also requires the binding of both G$\beta\gamma$ subunits (*16*−*19*), which are membrane-associated in vivo due to geranylgeranylation of the $\gamma$ subunit, and anionic phospholipids (*20*−*23*). G$\beta\gamma$ and phospholipids bind to the C-terminal PH domain of GRK2 (*19*, *23*−*25*) in a cooperative manner (*26*) and act synergisti-

† This work was supported by American Heart Association Scientist Development Grant 0235273N, National Institute of Health Grant HL071818, and a Research Corporation Cottrell Scholar grant to J.J.G.T., by National Science Foundation Grants MCB9728179 and MCB0315888 to R.S.-M., and by the College of Natural Sciences support to the Center for Structural Biology (University of Texas at Austin). The Advanced Light Source is supported by the Director, Office of Science, Office of Basic Energy Sciences, Materials Sciences Division, of the U.S. Department of Energy under Contract DE-AC03-76SF00098 at Lawrence Berkeley National Laboratory.

* To whom correspondence should be addressed. E-mail: tesmer@mail.utexas.edu. Telephone: (512) 471-5675. Fax: (512) 471-8696.

‡ The University of Texas at Austin.

§ Siena College.

|| National Institute of Diabetes and Digestive and Kidney Diseases.

[1] Abbreviations: AGC, protein kinase A, G, and C related; CHAPS, 3-[(3-cholamidopropyl)dimethylammonio]-1-propanesulfonate; DTT, dithiothreitol; EDTA, ethylenediaminetetraacetic acid; Endo-Asp-N, endoproteinase Asp-N; G protein, guanine nucleotide binding protein; Gα, heterotrimeric G protein α subunit; G$\beta\gamma$, heterotrimeric G protein $\beta$ and $\gamma$ subunits; GPCR, G protein-coupled receptor; GRK, G protein-coupled receptor kinase; GTP, guanosine 5′-triphosphate; HEPES, 4-(2-hydroxyethyl)-1-piperazineethanesulfonic acid; PH, pleckstrin homology; RGS, regulator of G protein signaling; RH, RGS homology; SDS, sodium dodecyl sulfate.

10.1021/bi050119q CCC: $30.25 
Published on Web 04/15/2005

cally toward the phosphorylation of activated receptors (*20*). Disruption of either the Gβγ or the phospholipid binding site greatly diminishes both agonist- and GRK2-dependent receptor phosphorylation in vivo and in vitro (*23*). Because the GRK2 binding site on Gβγ overlaps with those of inactive Gα subunits (*27*, *28*), the interaction of GRK2 with Gβγ serves as a convenient mechanism for targeting the kinase to recently activated receptors (*17*). Reports are conflicting as to whether Gβγ can directly influence the intrinsic kinase activity of GRK2. While Gβγ subunits stimulate GRK2-mediated phosphorylation of activated GPCRs roughly 10-fold in vitro (*17*, *18*, *29*), they stimulate phosphorylation of soluble substrates much more modestly, if at all (*15*, *17*, *20*, *29*, *30*). The latter results are often taken as evidence for the lack of direct activation of GRK2 by Gβγ and, instead, support the role of Gβγ in merely localizing GRK2 to the membrane.

Recently, we determined the atomic structure of GRK2 in a peripheral membrane complex with $G\beta_1\gamma_2$ (*28*). Formation of their complex required CHAPS detergent micelles, which solubilized the geranylgeranylated Gβγ subunits and enhanced the affinity between GRK2 and Gβγ (*31*). The structure confirmed that GRK2 consists of three principal domains. The N-terminal domain is homologous to that found in the *r*egulator of *G* protein *s*ignaling (RGS) family of proteins (*32*), which is a bilobed domain of 9−12 α-helices, referred to herein as the RGS homology (RH) domain (Figure 1A). The protein kinase domain of GRK2 is inserted in a loop between the α9 and α10 helices of the RH domain and is ∼32% identical in sequence to the catalytic subunit of protein kinase A (PKA) and other AGC kinases (*33*, *34*). The RH and kinase domains form a discontinuous interface, consisting of a contact between the "terminal lobe" of the RH domain and the small lobe of the kinase domain and a much smaller contact between the "bundle lobe" of the RH domain and the large lobe of the kinase domain (Figure 1A). The RH and kinase domains thereby form an integrated unit that is likely to be conserved in all GRKs. The C-terminal PH domain of GRK2 forms an extensive interface with the terminal lobe of the RH domain, and Gβγ appears to interact exclusively with the PH domain (Figure 1A). Thus, the three domains of GRK2 are intimately associated, with the orientation of each domain fixed with respect to each other so that each can perform a specific task in the desensitization of GPCR signaling at the membrane surface (*28*).

However, the GRK2−Gβγ structure does not resolve whether binding Gβγ alters the conformation of GRK2 or whether dissociation (or association) of the observed domain interfaces could play a role in the catalytic cycle of GRK2. Previous studies have suggested that the domains of GRK2 undergo reorganization upon binding Gβγ (*35*), and dissociation of domain interfaces is recognized in other modular kinases, such as Src family kinases, as they transition from inactive to active states (*36*, *37*). Herein we describe crystallographic and biochemical studies that assess how the binding of Gβγ affects the structure of GRK2 and provide evidence that the major domain interfaces of GRK2 remain associated during the activation of GRK2.

## EXPERIMENTAL PROCEDURES

*Sources*. FF heparin−Sepharose, heparin CL-6B−agarose, Superdex 200 preparative gel filtration media, and Source 15S cation-exchange resin were obtained from Amersham-Pharmacia. Clostripain and sodium cholate were obtained from Sigma-Aldrich, endoproteinase Asp-N (Endo-Asp-N) and Azocoll were from EMD Biosciences, 3-[(3-cholamidopropyl)dimethylammonio]-1-propanesulfonate (CHAPS) was from Anatrace, and GRK2-specific polyclonal antibodies were from Santa Cruz Biotechnologies.

*Expression and Purification of Proteins.* Bovine GRK2 was expressed in Sf9 insect cells and purified as previously described (*31*) using a baculovirus encoding a mutant (S670A) recombinant GRK2 to remove a MAP kinase phosphorylation site. Bovine $G\beta_1H_6\text{-}\gamma_2$, which is geranylgeranylated, and $G\beta_1H_6\text{-}\gamma_2$(C68S), whose geranylgeranylation site is ablated, were produced as previously described (*38*). Herein, these G proteins are referred to as Gβγ and $G\beta\gamma_{C68S}$, respectively.

*Crystallization of GRK2*. Crystals were grown in hanging drop vapor diffusion experiments at 4 °C in 4 μL hanging drops using 2 μL of well solution [100 mM HEPES, pH 7.5−8.0, 1 M NaCl, 1 M urea, 10−40 mM phosphoserine, pH 7.0, 5% (v/v) glycerol, and 9.5−11.5% PEG 8000] mixed with 2 μL of 15 mg/mL GRK2 that was purified in a buffer consisting of 20 mM HEPES, pH 8.0, 200 mM NaCl, and 2 mM DTT. Crystals grew over the course of 2 to 3 weeks and reached maximum dimensions of 0.75 × 0.25 × 0.35 mm.

*X-ray Diffraction Data Collection and Structure Determination*. Hanging drops containing GRK2 crystals were diluted twice with 2 μL of a cryoprotectant solution containing 75% well solution and 25% of a solution containing 20 mM HEPES, pH 8.0, in ∼100% ethylene glycol. Crystals were then transferred to a 50 μL drop of the cryoprotectant and allowed to equilibrate for 5 min before the crystals were flash frozen in liquid nitrogen. Diffraction maxima were collected at the Advanced Light Source beamline 8.2.1 on a Quantum 210 CCD detector at 100 K. High levels of diffuse scatter were observed in the diffraction images, indicating a large degree of mobility within the crystal lattice. Crystals belong to space group *P*2 with unit cell parameters of $a = 115.2$ Å, $b = 82.2$ Å, $c = 218.8$ Å, and $\beta = 95.6°$. With four subunits per asymmetric unit, the Matthews coefficient ($V_m$) is 3.2, corresponding to 62% solvent. The GRK2 crystal structure was solved by molecular replacement with the program MOLREP (*39*) using the structure of GRK2 from the GRK2−Gβγ complex (PDB code 1OMW) as a search model.

*Model Refinement and Analysis*. The model was refined using TLS and restrained refinement in REFMAC5 (*39*). Noncrystallographic symmetry (NCS) restraints were applied to the individual domains of GRK2 during refinement to allow for their relative motion. As conformational differences within individual domains became apparent, the restraints and NCS groups were adjusted accordingly. The drop in $R_{free}$ during refinement justified the use of NCS. Furthermore, the refined symmetry operators from 4-fold density averaging in the program DM (*40*) agree well with those relating equivalent domains in the final model. At the end of refinement, the NCS restraints were relaxed, leading to a 3% drop in $R_{work}$. However, $R_{free}$ increased and the stereochemical quality of the model decreased, so the model with tight NCS restraints was retained. The individual isotropic *B*-factor for each atom was fixed at 40 Å$^2$. Higher or lower

Table 1: Crystallographic and Refinement Statistics

| | |
|---|---|
| X-ray source | ALS beamline 8.2.1 |
| wavelength (Å) | 1.000 |
| resolution (Å) | 4.5 |
| spacegroup | *P*2 |
| cell constants (Å, deg) | $a = 115.2$, $b = 82.2$, $c = 218.8$, $\beta = 95.6$ |
| mosaicity (deg) | 0.4 |
| unique reflections | 24354 |
| average redundancy | 3.4 |
| $R_{sym}$ (%)[a] | 5.5 (45.6) |
| completeness (%)[b] | 99.6 (98.9) |
| $\langle I\rangle/\langle\sigma_I\rangle$ | 21.4 (2.5) |
| refinement resolution (Å) | 20−4.5 |
| total reflections | 23122 |
| protein atoms | 19846 |
| RMSD bond lengths (Å) | 0.015 |
| RMSD bond angles (deg) | 1.5 |
| $R_{work}$[c] | 23.5 |
| $R_{free}$[d] | 27.3 |

[a] $R_{sym} = \sum_{hkl}\sum_i|I(hkl)_i - I(hkl)|/\sum_{hkl}I(hkl)$, where $I(hkl)$ is the mean intensity of $i$ reflections after rejections. A $-1.0I/\sigma_I$ cutoff was applied. [b] Numbers in parentheses correspond to the highest resolution shell of data (4.66−4.5 Å). [c] $R_{work} = \sum_{hkl}||F_o(hkl)| - |F_c(hkl)||/\sum_{hkl}|F_o(hkl)|$; no $I/\sigma$ cutoff was used during refinement. [d] 5% of the truncated data set was excluded from refinement to calculate $R_{free}$.

*B*-factors did not affect map quality or *R*-factors. After each round of refinement, models were fit into $\sigma_A$-weighted electron density maps using O (*41*). Stereochemistry was monitored utilizing PROCHECK (*42*), and no residues are found in "disallowed" regions of the Ramachandran plot. Disordered regions in each molecule are similar yet distinct from those of the GRK2−G$\beta\gamma$ structure and include the N-terminus (residues 1−28), the "nucleotide gate" of the kinase domain (residues 476−493), the $\beta1-\beta2$ loop of the PH domain (residues 571−573), and the C-terminus (residues 657−689). Residues 543−551 in the RH−PH linker are disordered in the D chain, most likely due to the fact that it would otherwise fall upon the crystallographic 2-fold axis and collide with a symmetry-related D chain. Analysis of the conformational variance among the GRK2 soluble monomers and GRK2−G$\beta\gamma$ structure was performed utilizing the programs Swiss-PDB Viewer (*43*) and ESCET (*44*, *45*). To create movies that "morph" between the various structures of GRK2, all GRK2 molecules were superimposed upon their kinase domains (residues 185−512), and intermediate structures were generated via adiabatic mapping utilizing CNS (*46*, *47*). These structures were then animated into a movie with the program PyMOL (*48*). Data collection and refinement statistics are listed in Table 1. Coordinates and structure factors are deposited at the Protein Data Bank with accession code 1YM7.

*Site-Directed Mutagenesis*. Minor modifications of the QuikChange mutagenesis (Stratagene) manufacturer's protocol were used to generate site-directed mutations in pcDNA3-GRK2 (*49*). The GRK2 portion of each construct was sequenced for verification.

*COS-1 Cell Transient Transfection.* In three independent experiments, COS-1 cells were grown at 37 °C to 50−80% confluence on 6 cm dishes and were transfected with 4 $\mu$g of plasmid DNA using Fugene-6 (Roche). After 48 h, cells were washed twice in lysis buffer (20 mM Tris-HCl, pH 8.0, 150 mM NaCl, 1 mM EDTA) and scraped into 0.4 mL of 20 mM HEPES, pH 7.2, 10 mM EDTA, 0.02% Triton X-100, 0.5 mM PMSF, 20 $\mu$g/mL leupeptin, and 100 $\mu$g/mL benzamidine. Soluble fractions were prepared from lysates by sonication followed by centrifugation for 10 min at 40000*g*. The protein concentration was determined by Bradford assay using $\gamma$-globulin as a standard and then adjusted to 1 mg/mL with lysis buffer.

To assess GRK2 expression, 10 $\mu$g of soluble lysate was analyzed on 8% SDS polyacrylamide gels alongside a 2−60 ng dilution series of GRK2 purified from Sf9 insect cells. Proteins were transferred to nitrocellulose, probed with GRK2-specific polyclonal antibodies (dilution of 1:10000), and incubated with peroxidase-conjugated secondary antibody. The immunoblots were developed by chemiluminescence using SuperSignal West Pico (Pierce). Both lysate and dilution series blots were measured on the same piece of film. A standard curve was generated from the dilution series, and the expression level of wild-type and mutant GRK2 was interpolated using NIH Image. Under the conditions described, endogenous GRK2 could not be visualized. Statistical significance was assessed by repeated-measures ANOVA with a Tukey's post test using the program Prism-Graphpad.

*Kinase Activity of Transiently Expressed Mutants*. Lysates from cells transfected with pcDNA3 alone, pcDNA3-GRK2, or pcDNA3-mutant GRK2 were assayed for their ability to phosphorylate dark-adapted and light-activated rhodopsin in urea-washed rod outer segment membranes, as previously described (*23*) with the modifications described below. Protein from transfected cell supernatants (6 $\mu$g) was incubated with 20 mM Tris-HCl, pH 7.5, 2 mM EDTA, 7.5 mM $MgCl_2$, 200 $\mu$M ATP, [$\gamma$-$^{32}$P]ATP (0.2 cpm/fmol), and 10 $\mu$M rhodopsin for 3 min at 30 °C in the dark or in room light in a 20 $\mu$L reaction. Reactions were quenched by the addition of 20 $\mu$L of SDS sample buffer, incubated for 30 min at 60 °C, and then resolved by 10% SDS−PAGE. Rhodopsin bands were then excised, and the extent of $\gamma$-$^{32}$P incorporation was measured by liquid scintillation. Background counts from pcDNA-transfected cells were subtracted from all measurements.

*Protease Protection Assays*. In pilot experiments, 0.05 unit of clostripain/mg of GRK2 at 25 °C and 23.3 units of Endo-Asp-N/mg of GRK2 at 30 °C yielded nearly complete cleavage of the full-length GRK2 protein overnight and these were used for subsequent protection assays. Major proteolytic fragments generated over the course of each digestion were identified by MALDI-TOF mass spectrometry and, in the case of clostripain, N-terminal sequencing. For the clostripain protection assay, a 50 $\mu$L master stock was prepared which contained 30 $\mu$M (120 $\mu$g) GRK2 in reaction buffer (20 mM HEPES, pH 8.0, 200 mM NaCl, and 2 mM DTT). CHAPS, as indicated, was added to a final concentration of 10 mM, taking into account the CHAPS already present in G$\beta\gamma$, if present (Figure 3). For assays that also included G proteins, 100 $\mu$g of either G$\beta\gamma$ or G$\beta\gamma_{C68S}$ was added to a final concentration of 40 $\mu$M. Endo-Asp-N digests were prepared similarly, except that the master stock was 30 $\mu$L, the GRK2 concentration was 50 $\mu$M, and 130 $\mu$g of G$\beta\gamma$ or G$\beta\gamma_{C68S}$ was added (final concentration of 75 $\mu$M). Protein concentrations were determined by Bradford using bovine serum albumin as a standard. After addition of protease, the reaction was divided into 8 $\mu$L aliquots. At each time point, proteolysis was quenched through the addition of 8 $\mu$L of 4× SDS−PAGE sample buffer, and 12 $\mu$L of the resulting mix was separated on 10% SDS−polyacrylamide gels.

Because CHAPS conferred partial protection from proteolytic digestion of GRK2 from Endo-Asp-N, the activity of Endo-Asp-N was tested on a control substrate, Azocoll, in the presence or absence of 10 mM CHAPS detergent. In three independent experiments performed in triplicate, Endo-Asp-N was actually 26 ± 8% more active in CHAPS.

*Sedimentation Equilibrium.* For equilibrium studies, the GRK2−Gβγ complex purification protocol (*31*) was modified because the presence of 1 mM ATP in the buffer would interfere with absorbance readings. GRK2 and Gβγ were mixed in a 1:1.5 molar ratio in complex buffer (20 mM HEPES, pH 8.0, 50 mM NaCl, 2 mM DTT, 10 mM CHAPS, 5 mM $MgCl_2$, and 1 mM ATP, pH 7.5) and incubated on ice for 30 min. The complex was then purified on two tandem Superdex 200 gel filtration columns preequilibrated in complex buffer lacking ATP. GRK−Gβγ purified in this manner appeared to be of a 1:1 ratio of GRK2 to Gβγ as assessed by SDS−PAGE, eluted from the columns at a similar molecular mass, and crystallized under the same conditions as the original complex (*31*). For comparison, Gβγ and GRK2 were each purified using the same gel filtration buffer.

Sedimentation equilibrium experiments were conducted at 4.0 °C on a Beckman Optima XL-A analytical ultracentrifuge. Samples were studied at two different loading concentrations and different rotor speeds. Data for the low-concentration samples were collected at a wavelength of 280 nm and rotor speeds of 6, 8, and 12 krpm, whereas data for the high-concentration samples were collected at 290 nm and rotor speeds of 6, 8, 10, 12, and 14 krpm. Data were acquired as an average of 16 absorbance measurements at a radial spacing of 0.001 cm. Equilibrium was usually achieved within 48 h. Data were initially analyzed in terms of a single ideal solute to obtain the buoyant molecular mass, $M_1(1 - \upsilon_1\rho)$, by fitting data from each scan to the equation $A_r = A_{o,1} \exp[HM_1(1 - \upsilon_1\rho)(r^2 - r_o^2)] + E$, where $A_{o,1}$ is the absorbance at a reference point $r_o$, $A_r$ is the absorbance at a given radial position $r$, $H = \omega^2/2RT$, $\omega$ is the angular speed in rads$^{-1}$, $R$ is the gas constant, $T$ is the absolute temperature, and $E$ is a small baseline correction. Residuals were calculated and plotted. Values of $M_1$ were obtained from the buoyant molecular mass, $M_1(1 - \upsilon_1\rho)$, and calculated using densities, $\rho$, at 4.0 °C obtained from standard tables. Values of $\upsilon_1$ were calculated on the basis of the amino acid composition (*50*). A partial specific volume $\upsilon$ of 1.1 cm$^3$/g was assumed for the geranylgeranyl group on the basis of data published for caprylic, capric, and lauric acids (*51*). In the case of CHAPS, a value of 0.732 cm$^3$/g was used (*52*). To obtain as much information about the GRK2−Gβγ sample as possible, a global analysis was performed using data collected at lower rotor speeds, namely, 6, 8, and 12 krpm for the low-concentration studies and 6, 8, and 10 krpm for the high-concentration studies. Data were analyzed in terms of three ideal solutes (a 1:1 mixture of free GRK2 and Gβγ, the GRK2−Gβγ complex, and the high molecular weight aggregate). The buoyant molecular mass for the smallest mass species was set to 18404 Da, which represents the weight average buoyant molecular mass of an assumedly equimolar mixture of GRK2 and Gβγ.[2] Equilibrium sedimentation data, including buoyant molecular masses and calculated molecular weights, are summarized in Table 3.

## RESULTS AND DISCUSSION

*The Crystal Structure of GRK2*. Comparison of the "soluble" GRK2 structure with that of the GRK2−Gβγ complex demonstrates that Gβγ binding does not lead to large structural changes in the domain organization of GRK2. There are four unique subunits of GRK2 (chains A−D) in the asymmetric unit of the GRK2 crystals, and each was located by molecular replacement using the structure of Gβγ-bound GRK2 as a search model. Superposition of each monomer in the refined structure with that of Gβγ-bound GRK2 ranges from a root mean squared deviation (RMSD) of 0.6 Å for equivalent $C^\alpha$ atoms for monomer D to 1.6 Å for monomer C (Table 2). The A and D monomers are statistically the same as Gβγ-bound GRK2 when one considers the estimated coordinate error of the model (~1 Å). One notable difference between the GRK2 and GRK2−Gβγ crystal structures is the loss of electron density for residues 657−668 at the C-terminus of the PH domain of unbound GRK2. This region corresponds to the end of αC and following coil, which interacts with Gβγ in the GRK2−Gβγ crystal structure. The NMR solution structure of the independently expressed PH domain also indicated that this region lacked defined structure (*25*). This region therefore becomes ordered only upon binding Gβγ.

In solution (*31*) and equilibrium sedimentation studies (see below), GRK2 exists as a monomer. In GRK2 crystals, two independent pseudosymmetric dimers (chain A with chain C, chain B with chain D, referred to as the "bundle lobe dimers") are formed (Figure 1B). These dimers are in turn associated at one end (between chains A and B, referred to herein as the "kinase/PH dimer") to form a V-shaped structure (Figure 1B) with overall pseudo-$C_2$ symmetry. The bundle lobe dimer interfaces each bury 1600 Å$^2$ of accessible surface area. They are formed by the α5 and α6 helices of the RH bundle lobe from each monomer, which pack together to form a 2-fold symmetric antiparallel four-helix bundle (Figures 1B and S1). Residues buried within this interface are generally hydrophobic and include those previously implicated in binding $G\alpha_q$ (*53*, *54*). The kinase−PH dimer interface is formed by contacts between the PH and kinase domains of each monomer (Figure 1B). The interface is hydrophilic in character and buries a total of 1400 Å$^2$ of accessible surface area.

The kinase domains of each GRK2 monomer and that of the GRK2−Gβγ complex appear to be identical (Table 2) and adopt a conformation similar to that of inactive structures of PKA or PKB (*55*, *56*). Upon superposition of kinase domains from each soluble chain of GRK2, it appears that the RH and PH domains move predominantly as a single unit with respect to the kinase domain. This observation is supported by superposition statistics (Table 2) and error-weighted difference distance matrix analysis (Figure S2). However, the RH and PH domains also appear to have a small degree of conformational flexibility with respect to each other (Figure 1B, Table 2, Movie S1). The RH domains of the A and D monomers form similar terminal−small lobe and bundle−large lobe interfaces as in Gβγ-bound GRK2

[2] Because analytical ultracentrifugation experiments determine weight average molecular masses, at low rotor speeds it is difficult to resolve Gβγ (experimental buoyant mass of 16670 Da) from GRK2 (experimental buoyant mass of 19860 Da).

Table 2: RMSD (Å) of Superposition for Domains from Five Independent Monomers of GRK2[a]

| monomer | A | B | C | D | G$\beta\gamma$ bound |
|---|---|---|---|---|---|
| A | | 0.58 (all)[b]<br>0.40 (RH + PH) | 1.1 (all)<br>0.34 (RH + PH) | 0.60 (all)<br>0.39 (RH + PH) | 0.75 (all)<br>0.60 (RH + PH) |
| B | 0.07 (RH)<br>0.05 (kinase)<br>0.04 (PH) | | 0.65 (all)<br>0.19 (RH + PH) | 0.92 (all)<br>0.32 (RH + PH) | 1.1 (all)<br>0.67 (RH + PH) |
| C | 0.08 (RH)<br>0.06 (kinase)<br>0.04 (PH) | 0.06 (RH)<br>0.06 (kinase)<br>0.05 (PH) | | 1.5 (all)<br>0.42 (RH + PH) | 1.6 (all)<br>0.69 (RH + PH) |
| D | 0.05 (RH)<br>0.05 (kinase)<br>0.04 (PH) | 0.06 (RH)<br>0.05 (kinase)<br>0.04 (PH) | 0.07 (RH)<br>0.06 (kinase)<br>0.04 (PH) | | 0.62 (all)<br>0.62 (RH + PH) |
| G$\beta\gamma$ bound | 0.54 (RH)<br>0.53 (kinase)<br>0.62 (PH) | 0.55 (RH)<br>0.52 (kinase)<br>0.61 (PH) | 0.55 (RH)<br>0.53 (kinase)<br>0.62 (PH) | 0.55 (RH)<br>0.52 (kinase)<br>0.62 (PH) | |

[a] Above the diagonal, all or two (RH and PH) domains were compared. Below the diagonal, individual domains were compared. The lower than expected values (<0.1 Å) for the individual domains of the GRK2 structure (A−D) reflect the fact that these domains were constrained to be the same during refinement, which was necessary given the low resolution of the data. The higher values upon comparison with the individual domains of the GRK2−G$\beta\gamma$ structure (bottom row) probably reflect real coordinate error, given that it is consistently higher across all domains. The significantly higher RMSD values in the top diagonal indicate that the individual domains can move significantly with respect to each other among the five independent structures (see also Figure S2). The RH + PH superpositions give much lower RMSD's than those comparing all three domains but higher RMSD's than those of the individual domains. This indicates that while these two domains move largely as a unit with respect to the kinase domain, they exhibit some subtle differences in their relative orientation among the five structures. [b] All: root mean squared deviation (RMSD) for 585 Cα atoms from all domains of GRK2 omitting the elbow region (543−551) between the RH and PH domains. RH/PH: RMSD for 285 Cα atoms from both the RH and PH domains omitting the elbow. RH: RMSD for 186 Cα atoms from the RH domain. Kinase: RMSD for 308 Cα atoms from the kinase domain. PH: RMSD for 99 Cα atoms from the PH domain.

(Figure 1A). However, the RH domains of the B and C chains have rotated ∼3° and ∼5°, respectively, away from the kinase domain (Figure 1C, Figure S2, Movie S1) and, thereby, disrupt the bundle−large lobe interface.

The PH domains of the four GRK2 monomers also exhibit a range of slightly different orientations with respect to the kinase domain (Figure 1C, Table 2). The D chain PH domain assumes a nearly identical orientation as that of G$\beta\gamma$-bound GRK2. Relative to the D chain, the A and B chain PH domains are identical and rotated ∼3° toward the kinase domain, while the C chain is rotated ∼5° (Figure 1C). In each case, the RH−PH interface is retained. These conformational differences are undoubtedly influenced by local crystal contacts. For example, the PH domains of the A and B monomers are probably positioned similarly because their kinase and PH domains constitute the kinase−PH dimer interface (Figure 1C).

The highest conformational variability among the four soluble GRK2 monomers is found within the linker region between the C-terminal portion of the bipartite RH domain and the PH domain (residues 540−555), which forms a sharp elbow at the end of the α11 helix (Figures 1A,C and S2). In the GRK2−G$\beta\gamma$ structure, this elbow region is poorly ordered, and therefore its conformational heterogeneity and its ability to be influenced by local crystal contacts (as in the D monomer; see Experimental Procedures) are not surprising.

The five independent structures of GRK2 (four from the soluble structure and one from the GRK2−G$\beta\gamma$ complex) provide five frames of a movie that depicts the known dynamic motions of GRK2 (Movie S1). We hypothesize that the binding of G$\beta\gamma$ selectively stabilizes the conformation of GRK2 observed in the GRK2−G$\beta\gamma$ crystal structure. However, as we have only one unique crystal structure of the GRK2−G$\beta\gamma$ complex, it remains possible that GRK2−G$\beta\gamma$ in solution could also exhibit a similar range of conformations.

*Site-Directed Mutagenesis of the Domain Interfaces of GRK2*. While all protein kinase domains are thought to attain similar conformations in their catalytically active form, many distinct structures define their inactive states (*57*). The two crystal structures of GRK2 demonstrate that the kinase domain of GRK2, in both its soluble and G$\beta\gamma$-associated forms, assumes an inactive conformation with the small and large lobes splayed ∼12° apart compared with the active conformations of PKA and PKB (*55*, *56*). The crystal structure of GRK2 also shows that the binding of G$\beta\gamma$ has no apparent effect on the overall domain organization of GRK2. However, the major activating step for all GRKs appears to be the binding of an activated GPCR, and thus both the soluble and G$\beta\gamma$-bound structures of GRK2 represent relatively inactive states of the kinase. Because the terminal and bundle lobes of the GRK2 RH domain assume positions that are similar to that of the SH3 and SH2 domains, respectively, in Src family kinases, we wished to test whether receptor-mediated activation of GRK2 involves dissociation of the domain interfaces of GRK2. If so, mutational disruption of the domain interfaces could lead to a constitutively active enzyme, as does displacement of the SH3 or SH2 domains in Src family kinases (*36*, *37*). If the observed domain interfaces of GRK2 are instead crucial for the enzymatic activity or fold of GRK2, then one would expect these mutant proteins to be less active or to express at greatly diminished levels.

The first set of mutants test the role of residues within the α10 helix of the RH terminal lobe, which contacts a similar region of the kinase small lobe as does the SH2−kinase domain linker of inactive Src (Figure 1A). Glu520 is nearly invariant among GRKs and forms a buried salt bridge at the interface. When transiently expressed in COS-1 cells,

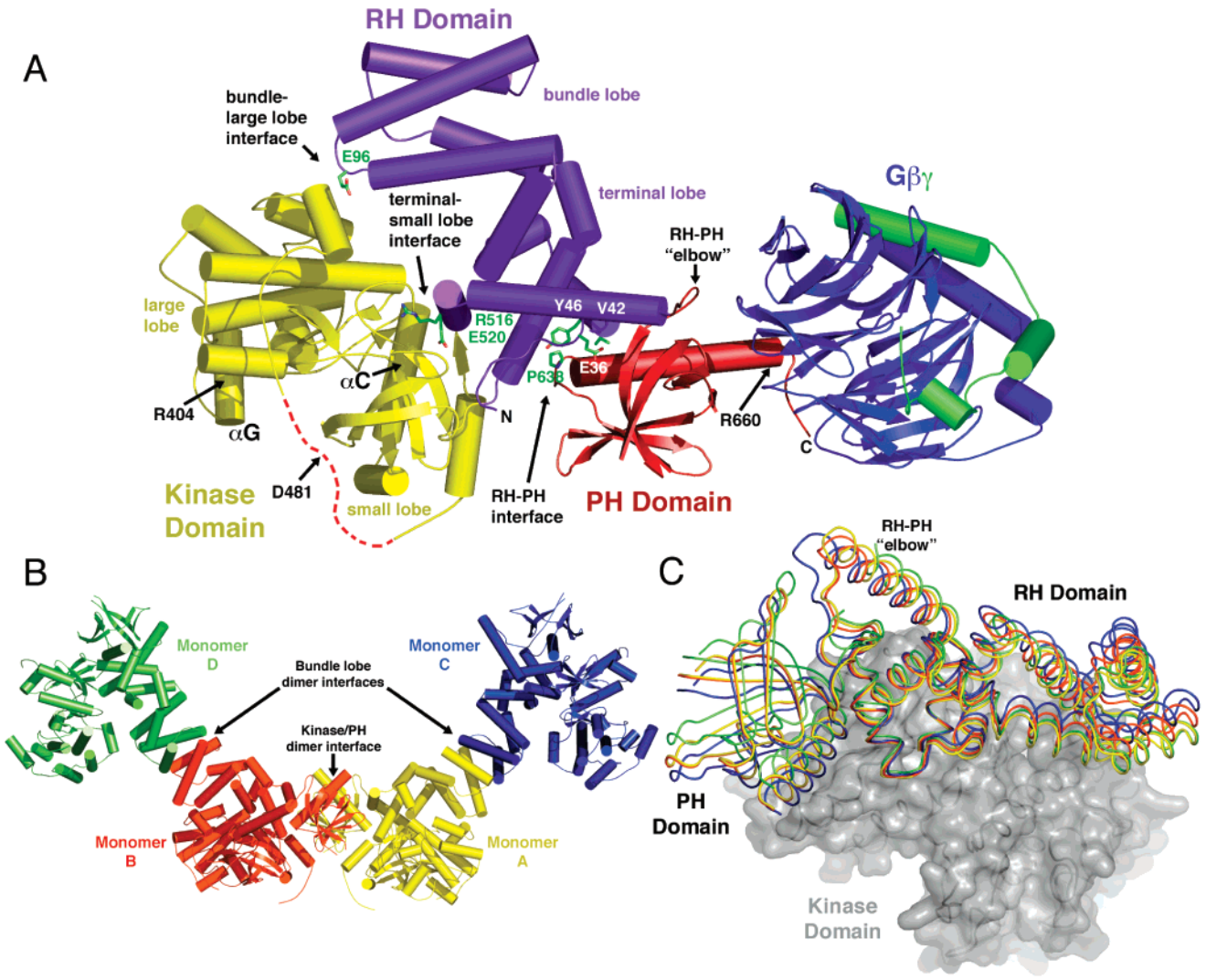


FIGURE 1: Atomic structures and conformational changes of GRK2. (A) Structure of the peripheral membrane complex of GRK2 with Gβγ (*28*) from the perspective of the cell membrane. The RH, kinase, and PH domains of GRK2 are colored purple, yellow, and red, respectively, while Gβγ is colored blue and green. The disordered nucleotide gate of GRK2 is shown as a red dashed line. The RH domain has two subdomains referred to herein as the terminal and bundle lobes, whereas the kinase domain is comprised of small and large lobes. The RH and kinase domains form two distinct interfaces. The first and larger interface is between the terminal lobe of the RH domain and the small lobe of the kinase domain (the terminal−small lobe interface; 1500 Å$^2$ total buried accessible surface area). The second is between the bundle lobe and the large lobe (the bundle−large lobe interface; 250 Å$^2$ total buried accessible surface area). The terminal lobe of the RH domain also forms an extensive hydrophobic interface with the PH domain (the RH−PH interface; 1400 Å$^2$ total buried accessible surface area). Stick models of domain interface residues targeted by site-directed mutagenesis in this study are shown with green carbons. The approximate positions of Arg404 in the αG helix of the kinase domain and Arg660 in the extended portion of the αC helix of the PH domain, which are targeted by clostripain, are indicated. Asp481 is located in the nucleotide gate and targeted by Endo-Asp-N. The N- and C-termini of GRK2 are labeled N and C. (B) Four unique monomers of GRK2 are found within the asymmetric unit of the soluble GRK2 crystals. Monomer A is colored yellow, monomer B red, monomer C blue, and monomer D green. Two distinct dimer interfaces are evident: those formed by the A:C and B:D monomers (the bundle−lobe dimer interfaces) and that formed by the A:B monomers (the kinase−PH dimer interface). Because the kinase−PH dimer interface happens to be perpendicular and adjacent to the crystallographic 2-fold axis, the four GRK2 chains form half of a $D_2$ pseudosymmetric octamer. (C) Domain motions among the four monomers of soluble GRK2, with the kinase domain shown as a gray, semitransparent surface. Monomers were superimposed via their kinase domains, which have invariant structure among all four soluble monomers and Gβγ-bound GRK2 (Table 2). The color of each chain is the same as in panel B.

the E520A substitution mutant led to a dramatic loss of GRK2 expression and similar loss in the ability to phosphorylate light-activated rhodopsin (Figure 2A−C). Arg516 is conserved only in the GRK2/3 subfamily and makes several contacts with the small lobe of the kinase domain, including with residues that would directly interact with the substrate ATP. The R516A mutation expressed at 40% of wild type, but its activity toward rhodopsin was only slightly diminished. Neither mutation led to a GRK2 that could phosphorylate dark-adapted rhodopsin. Therefore, disruption and/or dissociation of the terminal−small lobe interface does not allow the enzyme to bypass the activation step conferred by the binding of an activated GPCR. The terminal−small lobe interface instead appears to play a role in protein stability, as evidenced by the levels of E520A and R516A expression.

The E96A mutation was designed to probe the smaller bundle−large lobe interface of GRK2 (Figure 1A). Glu96 is highly conserved, makes an electrostatic pair with Lys465 in the kinase domain, and buries a large amount of surface area within the interface. The E96A mutant expressed at a

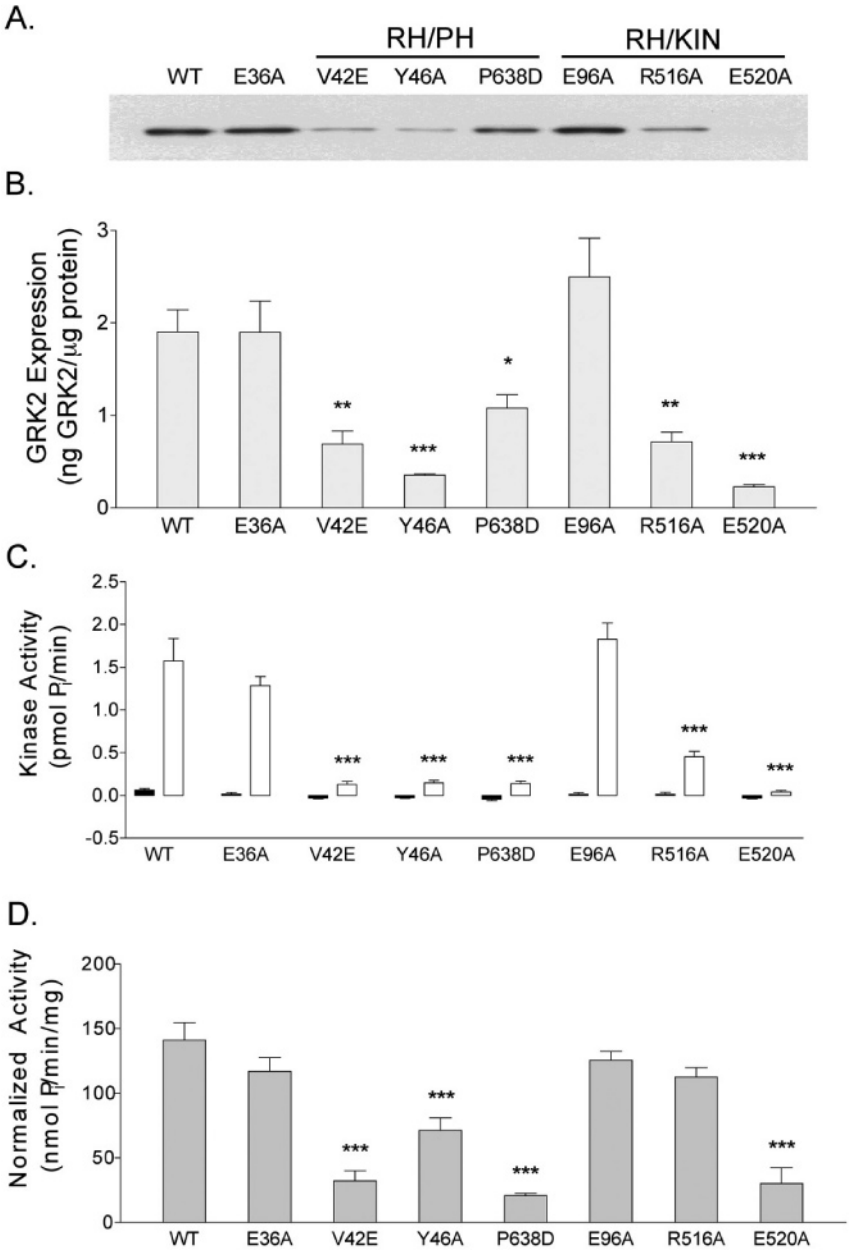


FIGURE 2: The observed domain interfaces of GRK2 are required for expression and activity. (A) Immunoblot of clarified lysates prepared from COS-1 cells transiently transfected with wild-type GRK2 and domain interface mutant constructs. (B) Quantitation of expressed GRK2. Serial dilutions of purified GRK2 were detected by immunoblotting and used to estimate expression from lysates. The means ± standard deviations of three independent transfection experiments are shown. Repeated-measures ANOVA was used to compare statistical significance relative to wild-type GRK2. Key: *, $p < 0.05$; **, $p < 0.01$; ***, $p < 0.001$. (C) GRK2 catalytic activity in domain interface mutants. Lysates from transfected COS-1 cells (6 $\mu$g) were mixed with 10 $\mu$M dark-adapted rhodopsin for 3 min at 30 °C either in the dark (dark bars) or after illumination (light bars). Endogenous kinases accounted for 0.13 and 0.23 pmol of $P_i$ transferred/min in the dark and light, respectively. Values represent means ± standard errors for six experiments derived from three different lysates, wherein each measurement was carried out in duplicate. Negative values reflect the observation that phosphorylation of rhodopsin in the dark was lower in mutant lysates than in the vector-transfected lysates. (D) Specific activity of interface mutants, as estimated from the experiments represented in the previous panels. Values represent means ± standard errors.

slightly greater level than wild-type GRK2, but its specific activity is statistically identical (Figure 2D). Maintenance of the bundle−large lobe interface may not be of great consequence for folding or expression of GRK2. Moreover, the soluble GRK2 crystal structure shows that this interface is labile in two of the GRK2 monomers (chains B and C).

To assess the importance of the RH−PH interface, we produced disruptive mutations of hydrophobic residues buried within the RH−PH interface (V42E, Y46A, and P638D) (Figure 1A). The V42E and Y46A mutants expressed poorly at 40% and 20% the level of wild type, respectively. While the specific activity of V42E was 25% of wild type, Y46A retained 50% of the intrinsic kinase activity. The P638D mutation is notable because it expressed reasonably well (60% of wild type) but had the lowest intrinsic kinase activity (15%) of all mutants tested. The fact that a residue in the PH domain can have a dramatic effect on the activity of the relatively remote kinase domain suggests that modulation of the RH−PH interface can indeed influence kinase activity. Therefore, interactions between the PH domain and phospholipids/G$\beta\gamma$ could allosterically modulate the activity of the kinase domain, at least in principle.

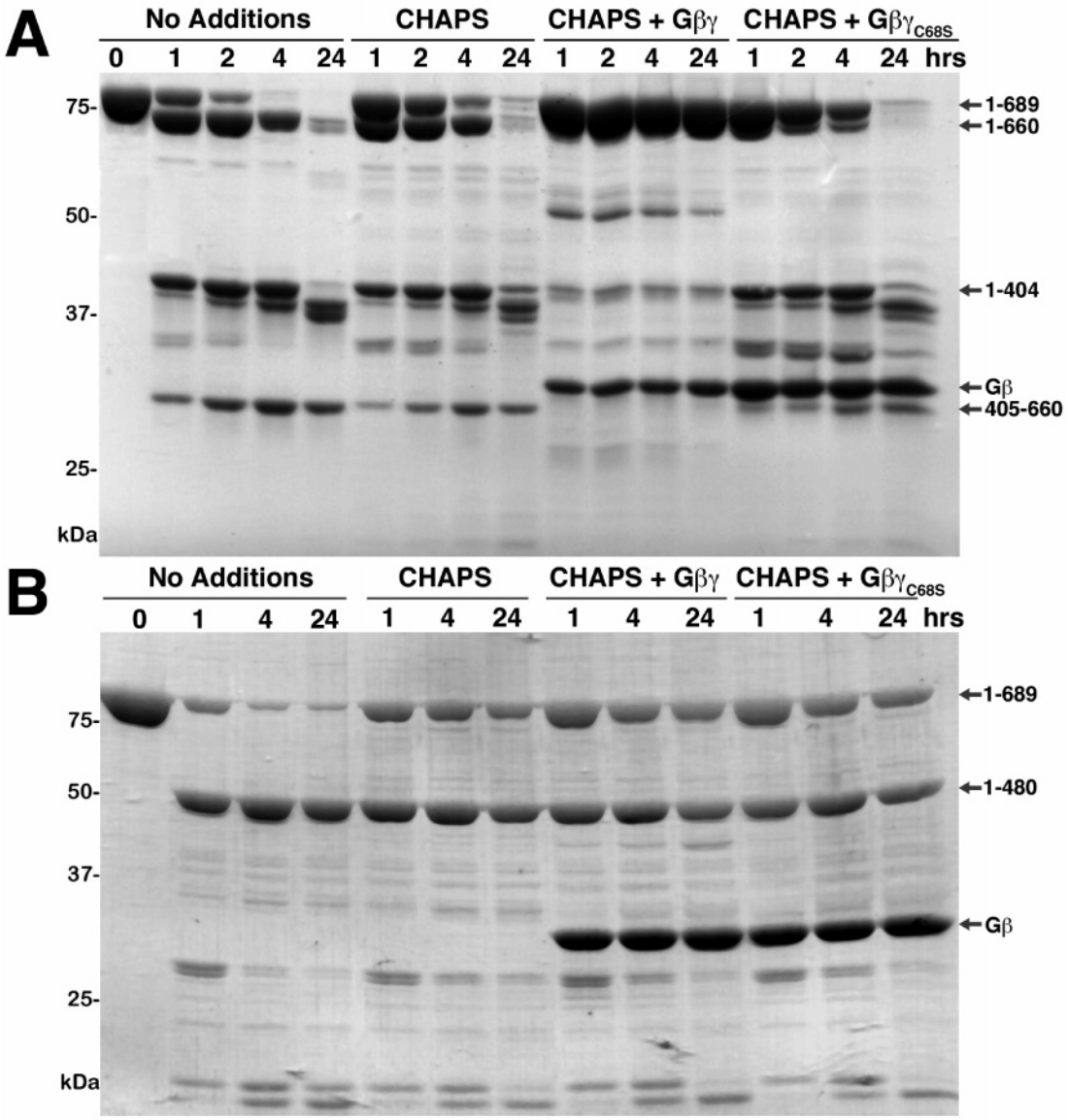


FIGURE 3: Protease protection studies. (A) G$\beta\gamma$ and, to a lesser extent, G$\beta\gamma_{C68S}$ protect GRK2 from digestion by clostripain. Recombinant GRK2 was mixed with either 10 mM CHAPS, CHAPS plus G$\beta\gamma$ (1.3 mol of G$\beta\gamma$/mol of GRK2), or CHAPS plus G$\beta\gamma_{C68S}$, as described in the Experimental Procedures. Reactions were initiated by the addition of clostripain and stopped after 1, 2, 4, and 24 h and then visualized on a 10% SDS−PAGE gel by Coomassie blue staining. Proteolytic fragments of GRK2 (right column) were identified through a combination of N-terminal sequencing and MALDI-TOF mass spectrometry. The left column reflects the positions of broad-range molecular mass standards (Bio-Rad). (B) CHAPS micelles and G$\beta\gamma$ protect GRK2 from digestion by Endo-Asp-N. Digests were performed similarly to those in panel A except using 1, 4, and 24 h time points and 1.5 mol of G$\beta\gamma$/mol of GRK2. The gels shown are representative of at least three independent experiments.

Glu36 is at the periphery of the RH−PH interface and is in close proximity to Arg578 in the PH domain, a residue previously suggested to be important for phospholipid-mediated activation of GRK2 (*23*). The E36A substitution had no effect on GRK2 expression or kinase activity (Figure 2), suggesting that phospholipid binding by the PH domain does not communicate to the RH domain through an interdomain Glu36−Arg578 salt bridge.

In summary, substitution of residues that are buried in domain interfaces (V42E, Y46A, R516A, E520A, P638D) led to reduced expression and lower kinase activity. Mutation of more solvent exposed residues, such as E96A or E36A, had no observed effect. Even when the amino acid substitution is somewhat tolerated, as in the case of P638D, perturbation of the interface does not lead to a more active kinase, but rather a defective one. Taken together with the GRK2−G$\beta\gamma$ and GRK2 crystal structures, these results all suggest that the terminal−small lobe and the RH−PH interfaces are essential to the fold and stability of GRK2. The fact that domain interface mutants of GRK2 do not lead to enhanced activity toward rhodopsin in the presence or absence of light suggests that GPCRs do not activate GRKs by freeing constraints imposed by these interfaces.

*Protease Protection Assays*. Crystal structures reveal only static images of proteins. Protease protection assays were therefore used to identify flexible regions of GRK2 that might be influenced by the presence or absence of G$\beta\gamma$ (Figure 3). Two proteases were employed: clostripain, which cuts peptide bonds C-terminal to arginine residues, and Endo-Asp-N, which cuts prior to aspartic acid residues. Digestion of GRK2 with clostripain (0.05 unit/mg of GRK2) for 4 h generated prominent 46 and 30 kDa fragments by SDS−

Table 3: Sedimentation Equilibrium Measurements on GRK2 and G$\beta\gamma$ and Their Complex

| sample | $M(1 - \upsilon\rho)$/Da[a] | $\upsilon$/cm$^3$ g$^{-1}$ [b] | $M_{exp}$/Da[c] | $M_{calc}$/Da[d] | $n$[e] | CHAPS[f] |
|---|---|---|---|---|---|---|
| GRK2 | 19840 ± 1320 | 0.7413 | 77580 ± 5160 | 79630.8 | 0.97 ± 0.06 | − |
| G$\beta\gamma$ | 16670 ± 1120 | 0.7283 | 62240 ± 4230 | 47478.5 | 1.30 ± 0.09 | 24 ± 7 |
| GRK2−G$\beta\gamma$ | 42260 ± 3520 | 0.7365 | 161760 ± 13470 | 127109.3 | 1.16 ± 0.10 | 35 ± 22 |
| CHAPS | 163 | 0.732 | | 614.9 | | |
| geranylgeranyl | −30 | 1.1 | | 289.5 | | |

[a] Experimentally determined buoyant molecular masses. In the case of GRK2 and G$\beta\gamma$ data represent average values obtained from a single ideal solute analysis using data collected at rotor speeds of 6−14 krpm and two loading concentrations. In the case of their complex, data represent the average of three multispeed global analyses carried out as described. Buoyant molecular masses for the CHAPS and geranylgeranyl tail of G$\gamma$ represent calculated values. [b] Calculated partial specific volumes based on the amino acid composition, including the contribution of the geranylgeranyl tail. The value for CHAPS has been determined (*52*), and the value for the geranylgeranyl was calculated as described in the text. [c] Experimentally determined molecular masses, including contributions from CHAPS. [d] Calculated molecular masses based on the amino acid composition and geranylgeranyl contributions. [e] Stoichiometry. [f] Estimated number of bound CHAPS molecules.

PAGE. These fragments were subsequently identified by MALDI-TOF mass spectrometry and N-terminal sequencing as comprising residues 1−404 and residues 405−660 (Figures 1A and 3A). Arg404 is found within the αG helix of the kinase domain, which is adjacent to the presumed polypeptide binding channel. Arg660 is found in the extended C-terminal helix of the PH domain, close to the surface of G$\beta\gamma$ in the GRK2−G$\beta\gamma$ complex (*28*). Digestion of GRK2 with Endo-Asp-N (23.3 units/mg of GRK2) generated a prominent and stable 55 kDa fragment by SDS−PAGE (Figure 3B). MALDI-TOF analysis of the mixture identified this fragment as residues 1−480. Another fragment corresponding to residues 481−689 of GRK2 was also identified, although it is not prominent in SDS−PAGE gels (Figure 3B). Endo-Asp-N therefore cuts GRK2 within the nucleotide gate region of GRK2 (Figure 1A), which is disordered in the soluble and G$\beta\gamma$-bound crystal structures of GRK2. The C-terminal Endo-Asp-N fragment of GRK2, which includes the PH domain, is either completely digested or is nicked at multiple sites such that it generates bands at low molecular mass by SDS−PAGE (Figure 3B).

CHAPS micelles (10 mM) had little effect on digestion of GRK2 by clostripain. As expected, the binding of either geranylgeranylated G$\beta\gamma$ or the soluble mutant G$\beta\gamma_{C68S}$ protected the Arg660 cut site of GRK2, most likely by stabilizing the structure of the extended C-terminal helix of the GRK2 PH domain. Interestingly, geranylgeranylated G$\beta\gamma$, but not G$\beta\gamma_{C68S}$, also protected GRK2 from cleavage at Arg404, rendering the GRK2−G$\beta\gamma$ complex nearly impervious to cleavage by clostripain under our assay conditions. Therefore, the geranylgeranylation of G$\beta\gamma$, along with the prerequisite detergent micelles, leads to protection of a site more than 80 Å away from the G$\beta\gamma$ binding site of GRK2 (Figure 1A).

Unlike in the case of clostripain, 10 mM CHAPS appeared to protect the nucleotide gate of GRK2 from cleavage by Endo-Asp-N (compare the disappearance of full-length GRK2 in Figure 3B). The addition of G$\beta\gamma_{C68S}$ or G$\beta\gamma$ appeared to slightly increase protection[3] (Figure 3B). Digestions of a control substrate revealed that the protease was more active in the presence of CHAPS, and therefore the protection is best explained by a partial ordering of the nucleotide gate of GRK2, apparently resulting from association with detergent micelles. Although we do not observe the nucleotide gate in our crystal structures, it is predicted to reside in close proximity to the plasma membrane in vivo (*28*).

Phospholipid vesicles (phosphatidylcholine and phosphatidylinositol sonicated in a ratio of 100:10 mM, final concentration), 10 mM $Mg^{2+}$ATP, 1 mM mastoparan, and a soluble peptide substrate (RRREEEEESAAA)[4] failed to provide significant protection of GRK2 from either protease (data not shown). The inability of these ligands to protect is not surprising given our inability to observe these ligands in cocrystallizations with GRK2 or GRK2−G$\beta\gamma$.

*Equilibrium Sedimentation Studies*. Two explanations for the observed protective effects of G$\beta\gamma$ in the clostripain protection assays are that GRK2 could either oligomerize when in complex with G$\beta\gamma$, leading to sequestration or stabilization of proteolytically sensitive sites, or that the CHAPS micelle, when recruited to GRK2 with the help of G$\beta\gamma$, assumes a size large enough to block access of the proteases to their cleavage sites. While CHAPS micelles are estimated to consist of 6−10 molecules under standard conditions (*58*), in some instances they can apparently be recruited to proteins in much larger numbers (*59*). To test these theories, GRK2, G$\beta\gamma$, and the GRK2−G$\beta\gamma$ complex were analyzed in a series of sedimentation equilibrium experiments, the results of which are summarized in Table 3. GRK2 does not form a high-affinity complex with G$\beta\gamma_{C68S}$ in either the presence or absence of 10 mM CHAPS (*31*). Therefore, equilibrium sedimentation experiments on this mixture are not feasible.

At lower concentration ($A_{280}$ = 0.90), GRK2 is monodisperse irrespective of the rotor speed (Figure 4A). Excellent fits to a single ideal solute model were obtained to yield a molecular mass of 78330 ± 3700 Da, indicating that the sample is monomeric ($n$ = 0.98 ± 0.05). Similar observations were made at higher concentration ($A_{280}$ = 1.14; 76990 ± 6600 Da; $n$ = 0.97 ± 0.08). Experiments on G$\beta\gamma$ at both lower and higher concentrations ($A_{280}$ = 0.96 and 1.5, respectively) show that the sample is also monodisperse with an average buoyant molecular mass of 16670 ± 1120 Da ($n$ = 1.30 ± 0.09) (Figure 4B), which is greater than predicted. The buoyant molecular mass difference of 3910 ± 1120 Da most likely reflects the binding of 24 ± 7 CHAPS molecules,

[3] Although it may not appear that 10 mM CHAPS protects differently than when G$\beta\gamma$ is present, gels loaded with less protein clearly indicate that inclusion of G$\beta\gamma$ protects GRK2 from Endo-Asp-N digestion more than CHAPS alone.

[4] RRRREEEEESAAA peptide at 4 mM partially protected GRK2 from clostripain digestion. However, because the EEEEESAAA peptide did not confer any protection, protection was most likely due to competition for the protease active site.

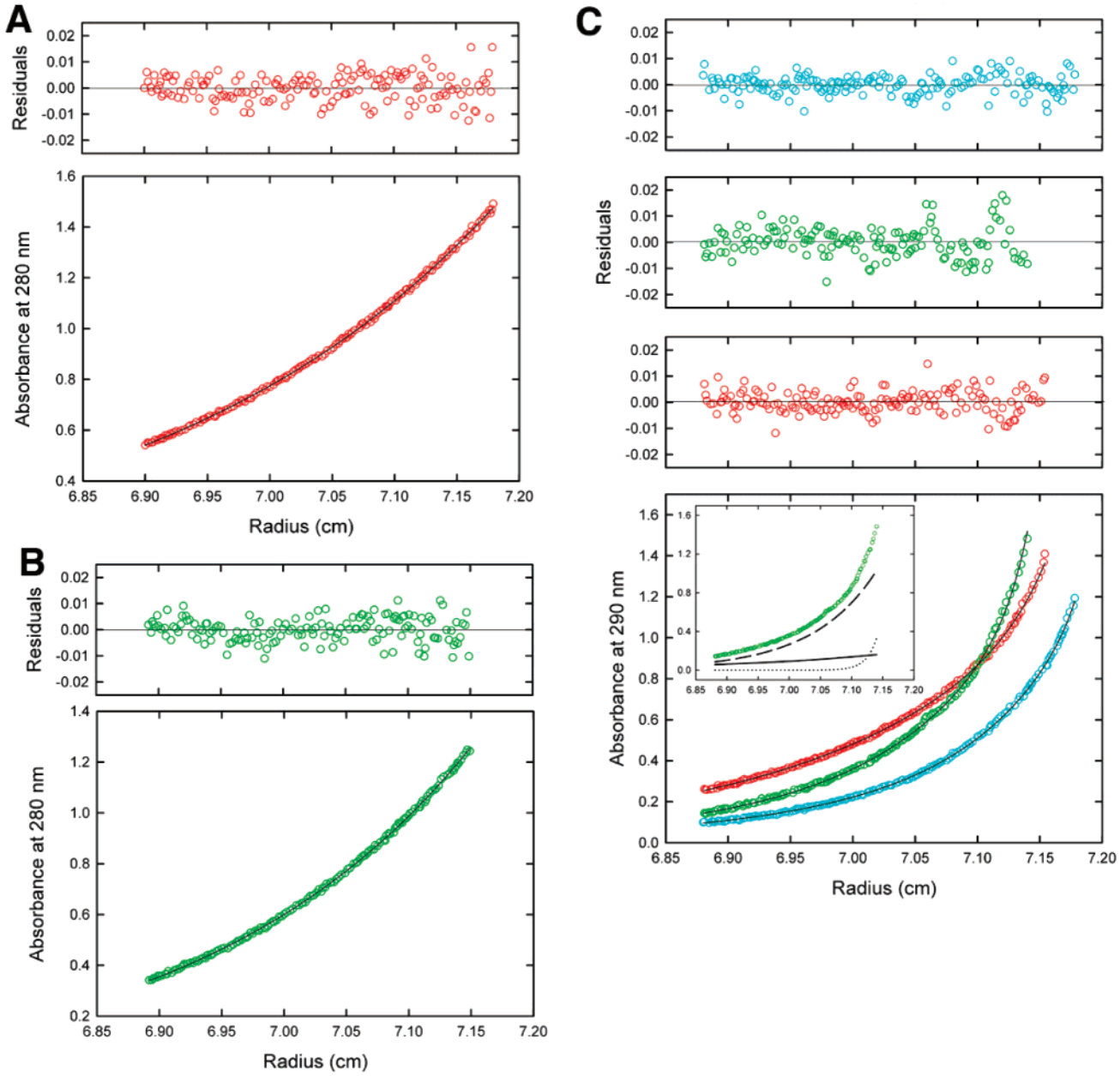


FIGURE 4: Sedimentation equilibrium studies of GRK2, Gβγ, and the GRK2−Gβγ complex. (A) GRK2 is a monomer. Sedimentation equilibrium profile at 280 nm and 4.0 °C for GRK2 loaded at an $A_{280}$ of 0.90 and collected at 8000 rpm. The lines through the data represent the best-fit analysis in terms of a single ideal solute, and the distributions of the residuals to this fit are shown in the panels above. (B) Gβγ is a monomer and binds 24 ± 7 CHAPS molecules. Sedimentation equilibrium profile at 280 nm and 4.0 °C for Gβγ loaded at an $A_{280}$ of 0.96 and collected at 8000 rpm. (C) GRK2 and Gβγ interact to form a 1:1 complex. Sedimentation equilibrium profiles at 290 nm and 4.0 °C for the GRK2−Gβγ complex loaded at an $A_{280}$ of 1.25 and collected at 6000 (red), 8000 (green), and 10000 (cyan) rpm. Note the apparent shift at 10000 rpm corresponding to the possible loss of higher molecular mass material. The lines through the data represent the weighted best-fit global analysis in terms of three noninteracting ideal solutes, in which one of the solutes represents the 1:1 contribution of free GRK2 and Gβγ. Residuals to this fit are shown in the panels above. The inset shows the relative contributions of the free GRK2 and Gβγ (solid line), 1:1 complex (dashed line), and aggregate (dotted line) to the experimental data collected at 8000 rpm.

which are presumably associated with the hydrophobic geranylgeranyl group of Gγ.

At a higher loading concentration ($A_{280}$ = 1.25), the GRK2−Gβγ complex is polydisperse and also contains free GRK2, Gβγ, and a higher order species, which reflects the presence of large aggregates present in miniscule amounts. On the basis of analysis of lower ($A_{280}$ = 0.80) and higher concentration data (Figure 4C), the GRK2−Gβγ complex has an average buoyant molecular mass of 42260 ± 3520 Da, which is 1.16 ± 0.10 times larger than expected, which indicates either that (i) within the error of the method the mass is identical to that of the 1:1 complex, (ii) the excess buoyant mass of 5730 ± 3520 Da corresponds to an excess of 35 ± 22 CHAPS molecules recruited to the complex, or (iii) a combination of (i) and (ii) in which the error results in fewer CHAPS species binding.

The maximum estimate of the number of CHAPS associated with the GRK2−Gβγ complex (57 per complex) could not, given its partial specific volume, constitute a sphere or even a bilayer large enough to span the distance from the geranylgeranyl group to block cleavage sites in the kinase domain. The additional CHAPS, if available to the complex,

could be enough to span both G$\beta\gamma$ and the GRK2 PH domain, which might explain why GRK2 forms a high-affinity complex with G$\beta\gamma$ but not G$\beta\gamma_{C68S}$ (*31*). We propose that the exquisite protection from clostripain afforded by G$\beta\gamma$ in CHAPS micelles is most easily explained through allosteric stabilization of the kinase domain.

*The Role of G$\beta\gamma$ and Domain Interfaces in the Activation of GRK2*. The crystal structure of soluble GRK2, with four copies of GRK2 in the asymmetric unit, demonstrates that the RH, kinase, and PH domains of GRK2 exhibit a limited degree of conformational flexibility. However, this mobility is small compared with domain rearrangements proposed for nonreceptor tyrosine kinases such as c-Src. Our mutagenesis studies indicate that the larger domain interfaces of GRK2 are integral to its fold, that domain reorganization does not occur upon binding G$\beta\gamma$, and that dissociation of the larger domain interfaces is not expected to occur during the activation of GRK2. Instead, our protease protection assays demonstrate that the binding of G$\beta\gamma$ could reinforce existing contacts between the RH and kinase domains. Interestingly, the bundle−large lobe interface (Figure 1A) remains intact in each of the GRK2 monomers that most closely resemble G$\beta\gamma$-bound GRK2, and this small interface could dampen dynamic motions of the large lobe (and hence the αG helix) and help to protect the kinase domain of GRK2 from clostripain digestion. Notably, stabilization of the αG helix upon ligand binding has also been observed in the distantly related C-terminal Src kinase (CSK) (*60*). Additional subtle alterations of the terminal−small lobe interface upon G$\beta\gamma$ binding, which cannot be assessed due to the low resolution of the GRK2 structure, could also have an effect on kinase activity. The region of the small lobe that interacts with the RH domain is well-known to be of regulatory significance for PKA and other protein kinases (*57*, *61*).

The geranylgeranyl group of G$\gamma$ is required for full protection of GRK2 from clostripain digestion (Figure 3A) and the formation of high-affinity complexes with GRK2 (*31*), even though it does not directly contact GRK2. The simplest explanation is that the C-terminal geranylgeranyl group of G$\gamma$ permits GRK2 to make contacts with the plasma membrane or detergent micelle in addition to its specific contacts with G$\beta$. Earlier studies showed that G$\beta\gamma$ was dispensable for full activity when an alternate route for tethering GRK2 to the membrane is introduced (*24*, *62*). This, when considered along with the fact that G$\beta\gamma_{C68S}$ cannot completely protect GRK2 from clostripain digestion, suggests that any activation and/or conformational stabilization of GRK2 by G$\beta\gamma$ is probably due to its synergistic interactions with the lipid bilayer or detergent micelles.

Our studies provide direct biophysical evidence that the binding of G$\beta\gamma$ in the presence of detergent micelles can have an effect on the conformation and dynamics of GRK2. However, these effects may or may not manifest themselves in kinetic assays, depending on the nature of the substrate. It is well documented that G$\beta\gamma$ and anionic phospholipids can stimulate the phosphorylation of activated GPCRs by GRKs. The fact that G$\beta\gamma$ fails to stimulate phosphorylation of soluble substrates to a similar extent has been used as evidence to support the hypothesis that G$\beta\gamma$- and phospholipid-mediated activation of GRK2 is due to localization rather than allostery. However, the soluble targets of GRK2 are relatively poor substrates and probably lack a second GRK2 binding site (a "docking site") that is distinct from their site(s) of phosphorylation. A docking site is required for efficient phosphorylation of receptors, a process that is up to several orders of magnitude more efficient than the phosphorylation of peptide substrates (*63*, *64*). Therefore, it is not unreasonable to expect that the phosphorylation of soluble substrates by GRKs will have a different rate-limiting step than that of membrane-bound, activated receptors. If true, elucidation of a molecular mechanism for G$\beta\gamma$-mediated activation using kinetic data from nonreceptor substrates is problematic.

Although GRK2 does not appear to be regulated by large domain rearrangements, its modular domains do appear to play important roles in the activation of GRK2 that correlate with what is known about the activation of other AGC kinases. For example, the N-terminal helix of PKA interacts with both the small and large lobes of the kinase domain and is thought to lend enhanced stability and to play a role in regulating conformational changes during the catalytic cycle (*61*, *65*). The RH domain of GRK2 binds to similar regions of both lobes of the kinase domain. Both PKB and protein kinase C are activated by phosphorylation of a C-terminal extension of their kinase domain (the "hydrophobic motif", which is absent in PKA) (*66*), which serves to tether the C-terminal extension onto the small lobe and stabilize the αC helix (*67*). GRK2 has a structurally equivalent extension, but phosphorylation is not necessary because the extension is permanently tethered to the small lobe by the C-terminal segment of the RH domain, which follows immediately after the motif (Figure 1A). Importantly, no phosphorylation of the GRK2 kinase domain is necessary for its function: even its activation loop is preordered. Apparently, the close association of the RH domain allows GRK2 to bypass several of the obligatory activation barriers that other AGC kinases are required to overcome. By circumventing these steps, GRK2−G$\beta\gamma$ is "primed" and waits for only one major stimulatory step: the binding of an activated GPCR.

With this in mind, it is striking that, among the five independent crystal structures of GRK2 (G$\beta\gamma$-bound GRK2 and the four monomers in the soluble GRK2 structure), the large and small lobes of the kinase appear to be locked in a nearly identical inactive conformation, wherein the large and small lobes of the kinase domain are splayed apart with respect to closed, active AGC kinase structures (*68*). The kinase domain in the crystal structure of GRK6 is similarly "open" even when bound to a nucleotide analogue (D. T. Lodowski, unpublished results). Therefore, the defining allosteric change exerted on GRK2 and other GRKs by hormone-occupied GPCRs most likely involves the ∼12° closure of its kinase domain into an active conformation similar to that of PKA (*56*), PKB (*55*), and presumably other AGC kinases. On the basis of the results of this study, it seems that major domain reorganization does not accompany this structural transition. The structure of a GRK in its active conformation and the molecular basis of the GPCR-induced allosteric transition are the subjects of current and future studies.

## ACKNOWLEDGMENT

The authors thank Dr. Robert J. Lefkowitz and his laboratory for Sf9 cell pellets containing recombinant GRK2

and Gβγ, Dr. Jeffrey L. Benovic for assistance in the preparation of bovine rod outer segments and for providing his laboratory as a venue for the training of undergraduate researchers, and Dr. Valerie Tesmer for critical reading of the manuscript. We also thank Siena College undergraduates Rebecca Bussert and Jamee Bresee for preparation of mutants and Christopher Davis for technical assistance.

## SUPPORTING INFORMATION AVAILABLE

Figure S1, electron density from a 4-fold averaged and solvent-flattened map at the A:C bundle lobe dimer interface; Figure S2, ESCET error correlated distance difference plot detailing the differences between the C and D monomers from the GRK2 structure; Movie S1, conformation changes among the four soluble GRK2 monomers from the soluble GRK2 structure and Gβγ-bound GRK2. This material is available free of charge via the Internet at http://pubs.acs.org.

## REFERENCES

1. Krupnick, J. G., and Benovic, J. L. (1998) The role of receptor kinases and arrestins in G protein-coupled receptor regulation, *Annu. Rev. Pharmacol. Toxicol. 38*, 289−319.
2. Pitcher, J. A., Freedman, N. J., and Lefkowitz, R. J. (1998) G protein-coupled receptor kinases, *Annu. Rev. Biochem. 67*, 653−692.
3. Luttrell, L. M., and Lefkowitz, R. J. (2002) The role of β-arrestins in the termination and transduction of G-protein-coupled receptor signals, *J. Cell Sci. 115*, 455−465.
4. Lohse, M. J., Benovic, J. L., Codina, J., Caron, M. G., and Lefkowitz, R. J. (1990) β-Arrestin: a protein that regulates β-adrenergic receptor function, *Science 248*, 1547−1550.
5. Attramadal, H., Arriza, J. L., Aoki, C., Dawson, T. M., Codina, J., Kwatra, M. M., Snyder, S. H., Caron, M. G., and Lefkowitz, R. J. (1992) β-arrestin2, a novel member of the arrestin/β-arrestin gene family, *J. Biol. Chem. 267*, 17882−17890.
6. Goodman, O. B., Jr., Krupnick, J. G., Santini, F., Gurevich, V. V., Penn, R. B., Gagnon, A. W., Keen, J. H., and Benovic, J. L. (1996) β-arrestin acts as a clathrin adaptor in endocytosis of the β2-adrenergic receptor, *Nature 383*, 447−450.
7. Daaka, Y., Luttrell, L. M., Ahn, S., Della Rocca, G. J., Ferguson, S. S., Caron, M. G., and Lefkowitz, R. J. (1998) Essential role for G protein-coupled receptor endocytosis in the activation of mitogen-activated protein kinase, *J. Biol. Chem. 273*, 685−688.
8. Perry, S. J., and Lefkowitz, R. J. (2002) Arresting developments in heptahelical receptor signaling and regulation, *Trends Cell Biol. 12*, 130−138.
9. Benovic, J. L., Strasser, R. H., Caron, M. G., and Lefkowitz, R. J. (1986) β-adrenergic receptor kinase: identification of a novel protein kinase that phosphorylates the agonist-occupied form of the receptor, *Proc. Natl. Acad. Sci. U.S.A. 83*, 2797−2801.
10. Benovic, J. L., DeBlasi, A., Stone, W. C., Caron, M. G., and Lefkowitz, R. J. (1989) β-adrenergic receptor kinase: primary structure delineates a multigene family, *Science 246*, 235−240.
11. Hata, J. A., and Koch, W. J. (2003) Phosphorylation of G protein-coupled receptors: GPCR kinases in heart disease, *Mol. Interventions 3*, 264−272.
12. Iaccarino, G., Lefkowitz, R. J., and Koch, W. J. (1999) Myocardial G protein-coupled receptor kinases: implications for heart failure therapy, *Proc. Assoc. Am. Physicians 111*, 399−405.
13. Onorato, J. J., Palczewski, K., Regan, J. W., Caron, M. G., Lefkowitz, R. J., and Benovic, J. L. (1991) Role of acidic amino acids in peptide substrates of the β-adrenergic receptor kinase and rhodopsin kinase, *Biochemistry 30*, 5118−5125.
14. Chen, C. Y., Dion, S. B., Kim, C. M., and Benovic, J. L. (1993) β-adrenergic receptor kinase. Agonist-dependent receptor binding promotes kinase activation, *J. Biol. Chem. 268*, 7825−7831.
15. Haga, K., Kameyama, K., and Haga, T. (1994) Synergistic activation of a G protein-coupled receptor kinase by G protein βγ subunits and mastoparan or related peptides, *J. Biol. Chem. 269*, 12594−12599.
16. Haga, K., and Haga, T. (1990) Dual regulation by G proteins of agonist-dependent phosphorylation of muscarinic acetylcholine receptors, *FEBS Lett. 268*, 43−47.
17. Pitcher, J. A., Inglese, J., Higgins, J. B., Arriza, J. L., Casey, P. J., Kim, C., Benovic, J. L., Kwatra, M. M., Caron, M. G., and Lefkowitz, R. J. (1992) Role of βγ subunits of G proteins in targeting the β-adrenergic receptor kinase to membrane-bound receptors, *Science 257*, 1264−1267.
18. Haga, K., and Haga, T. (1992) Activation by G protein βγ subunits of agonist- or light-dependent phosphorylation of muscarinic acetylcholine receptors and rhodopsin, *J. Biol. Chem. 267*, 2222−2227.
19. Kameyama, K., Haga, K., Haga, T., Kontani, K., Katada, T., and Fukada, Y. (1993) Activation by G protein βγ subunits of β-adrenergic and muscarinic receptor kinase, *J. Biol. Chem. 268*, 7753−7758.
20. Pitcher, J. A., Touhara, K., Payne, E. S., and Lefkowitz, R. J. (1995) Pleckstrin homology domain-mediated membrane association and activation of the β-adrenergic receptor kinase requires coordinate interaction with G βγ subunits and lipid, *J. Biol. Chem. 270*, 11707−11710.
21. Onorato, J. J., Gillis, M. E., Liu, Y., Benovic, J. L., and Ruoho, A. E. (1995) The β-adrenergic receptor kinase (GRK2) is regulated by phospholipids, *J. Biol. Chem. 270*, 21346−21353.
22. DebBurman, S. K., Ptasienski, J., Benovic, J. L., and Hosey, M. M. (1996) G protein-coupled receptor kinase GRK2 is a phospholipid-dependent enzyme that can be conditionally activated by G protein βγ subunits, *J. Biol. Chem. 271*, 22552−22562.
23. Carman, C. V., Barak, L. S., Chen, C., Liu-Chen, L. Y., Onorato, J. J., Kennedy, S. P., Caron, M. G., and Benovic, J. L. (2000) Mutational analysis of Gβγ and phospholipid interaction with G protein-coupled receptor kinase 2, *J. Biol. Chem. 275*, 10443−10452.
24. Koch, W. J., Inglese, J., Stone, W. C., and Lefkowitz, R. J. (1993) The binding site for the βγ subunits of heterotrimeric G proteins on the β-adrenergic receptor kinase, *J. Biol. Chem. 268*, 8256−8260.
25. Fushman, D., Najmabadi-Haske, T., Cahill, S., Zheng, J., LeVine, H., III, and Cowburn, D. (1998) The solution structure and dynamics of the pleckstrin homology domain of G protein-coupled receptor kinase 2 (β-adrenergic receptor kinase 1). A binding partner of Gβγ subunits, *J. Biol. Chem. 273*, 2835−2843.
26. Touhara, K. (1997) Binding of multiple ligands to pleckstrin homology domain regulates membrane translocation and enzyme activity of β-adrenergic receptor kinase, *FEBS Lett. 417*, 243−248.
27. Ford, C. E., Skiba, N. P., Bae, H., Daaka, Y., Reuveny, E., Shekter, L. R., Rosal, R., Weng, G., Yang, C. S., Iyengar, R., Miller, R. J., Jan, L. Y., Lefkowitz, R. J., and Hamm, H. E. (1998) Molecular basis for interactions of G protein βγ subunits with effectors, *Science 280*, 1271−1274.
28. Lodowski, D. T., Pitcher, J. A., Capel, W. D., Lefkowitz, R. J., and Tesmer, J. J. (2003) Keeping G proteins at bay: a complex between G protein-coupled receptor kinase 2 and Gβγ, *Science 300*, 1256−1262.
29. Kim, C. M., Dion, S. B., and Benovic, J. L. (1993) Mechanism of β-adrenergic receptor kinase activation by G proteins, *J. Biol. Chem. 268*, 15412−15418.
30. Carman, C. V., Som, T., Kim, C. M., and Benovic, J. L. (1998) Binding and phosphorylation of tubulin by G protein-coupled receptor kinases, *J. Biol. Chem. 273*, 20308−20316.
31. Lodowski, D. T., Barnhill, J. F., Pitcher, J. A., Capel, W. D., Lefkowitz, R. J., and Tesmer, J. J. (2003) Purification, crystallization and preliminary X-ray diffraction studies of a complex between G protein-coupled receptor kinase 2 and $G\beta_1\gamma_2$, *Acta Crystallogr., Sect. D: Biol. Crystallogr. 59*, 936−939.
32. Siderovski, D. P., Hessel, A., Chung, S., Mak, T. W., and Tyers, M. (1996) A new family of regulators of G-protein-coupled receptors?, *Curr. Biol. 6*, 211−212.
33. Hanks, S. K., and Hunter, T. (1995) Protein kinases 6. The eukaryotic protein kinase superfamily: kinase (catalytic) domain structure and classification, *FASEB J. 9*, 576−596.
34. Kostich, M., English, J., Madison, V., Gheyas, F., Wang, L., Qiu, P., Greene, J., and Laz, T. M. (2002) Human members of the eukaryotic protein kinase family, *Genome Biol. 3*, RESEARCH0043.
35. Sarnago, S., Roca, R., de Blasi, A., Valencia, A., Mayor, F., Jr., and Murga, C. (2003) Involvement of intramolecular interactions in the regulation of G protein-coupled receptor kinase 2, *Mol. Pharmacol. 64*, 629−639.
36. Gonfloni, S., Williams, J. C., Hattula, K., Weijland, A., Wierenga, R. K., and Superti-Furga, G. (1997) The role of the linker between

the SH2 domain and catalytic domain in the regulation and function of Src, *EMBO J. 16*, 7261−7271.
37. Moarefi, I., LaFevre-Bernt, M., Sicheri, F., Huse, M., Lee, C. H., Kuriyan, J., and Miller, W. T. (1997) Activation of the Src-family tyrosine kinase Hck by SH3 domain displacement, *Nature 385*, 650−653.
38. Kozasa, T. (1999) Purification of recombinant G protein α and $\beta\gamma$ subunits from Sf9 cells, in *G Proteins: Techniques of Analysis* (Manning, D. R., Ed.) pp 23−37, CRC Press LLC, Boca Raton, FL.
39. Winn, M. D. (2003) An overview of the CCP4 project in protein crystallography: an example of a collaborative project, *J. Synchrotron Radiat. 10*, 23−25.
40. Cowtan, K. (1994) DM: An automated procedure for phase improvement by density modification, *Joint CCP4 and ESF-EACBM Newsl. Protein Crystallogr. 31*, 34−38.
41. Jones, T. A., Zou, J. Y., Cowan, S. W., and Kjeldgaard, M. (1991) Improved methods for the building of protein models in electron density maps and the location of errors in these models, *Acta Crystallogr. A47*, 110−119.
42. Laskowski, R. A., MacArthur, M. W., Moss, D. S., and Thornton, J. M. (1993) PROCHECK: a program to check the stereochemical quality of protein structures, *J. Appl. Crystallogr. 26*, 283−291.
43. Kaplan, W., and Littlejohn, T. G. (2001) Swiss-PDB Viewer (Deep View), *Briefings Bioinf. 2*, 195−197.
44. Schneider, T. R. (2000) Objective comparison of protein structures: error-scaled difference distance matrices, *Acta Crystallogr., Sect. D: Biol. Crystallogr 56* (Part 6), 714−721.
45. Schneider, T. R. (2002) A genetic algorithm for the identification of conformationally invariant regions in protein molecules, *Acta Crystallogr., Sect. D: Biol. Crystallogr. 58*, 195−208.
46. Krebs, W. G., and Gerstein, M. (2000) The morph server: a standardized system for analyzing and visualizing macromolecular motions in a database framework, *Nucleic Acids Res. 28*, 1665−1675.
47. Brünger, A. T., Adams, P. D., Clore, G. M., DeLano, W. L., Gros, P., Grosse-Kunstleve, R. W., Jiang, J. S., Kuszewski, J., Nilges, M., Pannu, N. S., Read, R. J., Rice, L. M., Simonson, T., and Warren, G. L. (1998) Crystallography & NMR system: A new software suite for macromolecular structure determination, *Acta Crystallogr., Sect. D: Biol. Crystallogr. 54*, 905−921.
48. DeLano, W. (2002) The PyMOL Molecular Graphics System, DeLano Scientific, San Carlos, CA.
49. Sterne-Marr, R., Dhami, G. K., Tesmer, J. J., and Ferguson, S. S. (2004) Characterization of GRK2 RH domain-dependent regulation of GPCR coupling to heterotrimeric G proteins, *Methods Enzymol. 390*, 310−336.
50. Perkins, S. J. (1986) Protein volumes and hydration effects. The calculations of partial specific volumes, neutron scattering matchpoints and 280-nm absorption coefficients for proteins and glycoproteins from amino acid sequences, *Eur. J. Biochem. 157*, 169−180.
51. Durchschlag, H. (1986) Specific volumes of biological macromolecules and some other molecules of interest, in *Thermodynamic Data for Biochemistry and Biotechnology* (Hinz, H.-J., Ed.) pp 45−128, Springer-Verlag, Berlin.
52. Wagner, S. L., Dean, W. L., and Gray, R. D. (1984) Effect of a zwitterionic detergent on the state of aggregation and catalytic activity of cytochrome P-450LM2 and NADPH-cytochrome P-450 reductase, *J. Biol. Chem. 259*, 2390−2395.
53. Sterne-Marr, R., Tesmer, J. J., Day, P. W., Stracquatanio, R. P., Cilente, J. A., O'Connor, K. E., Pronin, A. N., Benovic, J. L., and Wedegaertner, P. B. (2003) G protein-coupled receptor kinase 2/$G\alpha_{q/11}$ interaction. A novel surface on a regulator of G protein signaling homology domain for binding G α subunits, *J. Biol. Chem. 278*, 6050−6058.
54. Day, P. W., Tesmer, J. J., Sterne-Marr, R., Freeman, L. C., Benovic, J. L., and Wedegaertner, P. B. (2004) Characterization of the GRK2 binding site of $G\alpha_q$, *J. Biol. Chem. 279*, 53643−53652.
55. Yang, J., Cron, P., Good, V. M., Thompson, V., Hemmings, B. A., and Barford, D. (2002) Crystal structure of an activated Akt/protein kinase B ternary complex with GSK3-peptide and AMP-PNP, *Nat. Struct. Biol. 9*, 940−944.
56. Madhusudan, Akamine, P., Xuong, N. H., and Taylor, S. S. (2002) Crystal structure of a transition state mimic of the catalytic subunit of cAMP-dependent protein kinase, *Nat. Struct. Biol. 9*, 273−277.
57. Huse, M., and Kuriyan, J. (2002) The conformational plasticity of protein kinases, *Cell 109*, 275−282.
58. Hjelmeland, L. M., Nebert, D. W., and Osborne, J. C., Jr. (1983) Sulfobetaine derivatives of bile acids: nondenaturing surfactants for membrane biochemistry, *Anal. Biochem. 130*, 72−82.
59. McGuire, A. M., Matsuo, H., and Wagner, G. (1998) Internal and overall motions of the translation factor eIF4E: cap binding and insertion in a CHAPS detergent micelle, *J. Biomol. NMR 12*, 73−88.
60. Hamuro, Y., Wong, L., Shaffer, J., Kim, J. S., Stranz, D. D., Jennings, P. A., Woods, V. L., Jr., and Adams, J. A. (2002) Phosphorylation driven motions in the COOH-terminal Src kinase, CSK, revealed through enhanced hydrogen−deuterium exchange and mass spectrometry (DXMS), *J. Mol. Biol. 323*, 871−881.
61. Herberg, F. W., Zimmermann, B., McGlone, M., and Taylor, S. S. (1997) Importance of the A-helix of the catalytic subunit of cAMP-dependent protein kinase for stability and for orienting subdomains at the cleft interface, *Protein Sci. 6*, 569−579.
62. Inglese, J., Koch, W. J., Caron, M. G., and Lefkowitz, R. J. (1992) Isoprenylation in regulation of signal transduction by G-protein-coupled receptor kinases, *Nature 359*, 147−150.
63. Fowles, C., Sharma, R., and Akhtar, M. (1988) Mechanistic studies on the phosphorylation of photoexcited rhodopsin, *FEBS Lett. 238*, 56−60.
64. Palczewski, K., Buczylko, J., Kaplan, M. W., Polans, A. S., and Crabb, J. W. (1991) Mechanism of rhodopsin kinase activation, *J. Biol. Chem. 266*, 12949−12955.
65. Smith, C. M., Radzio-Andzelm, E., Madhusudan, Akamine, P., and Taylor, S. S. (1999) The catalytic subunit of cAMP-dependent protein kinase: prototype for an extended network of communication, *Prog. Biophys. Mol. Biol. 71*, 313−341.
66. Newton, A. C. (2002) Regulation of the ABC kinases by phosphorylation: protein kinase C as a paradigm, *Biochem. J. 370*, 361−371.
67. Yang, J., Cron, P., Thompson, V., Good, V. M., Hess, D., Hemmings, B. A., and Barford, D. (2002) Molecular mechanism for the regulation of protein kinase B/Akt by hydrophobic motif phosphorylation, *Mol. Cell 9*, 1227−1240.
68. Taylor, S. S., Yang, J., Wu, J., Haste, N. M., Radzio-Andzelm, E., and Anand, G. (2004) PKA: a portrait of protein kinase dynamics, *Biochim. Biophys. Acta 1697*, 259−269.

BI050119Q